

Hyperfine structure of 2^3P levels of heliumlike ions

W. R. Johnson

Department of Physics, Notre Dame University, Notre Dame, Indiana 46556

K. T. Cheng

University of California, Lawrence Livermore National Laboratory, Livermore, California 94550

D. R. Plante

Center for Information Technology, Stetson University, DeLand, Florida 32720

(Received 19 November 1996)

A systematic calculation of the hyperfine structure of 2^3P levels of heliumlike ions is presented. Reduced matrix elements of the magnetic-dipole hyperfine operator between substates of the $2^{1,3}P$ states are evaluated using relativistic configuration-interaction wave functions that account for both Coulomb and Breit interactions. These matrix elements, together with the energy intervals $\Delta E_{10} = E(2^3P_1) - E(2^3P_0)$, $\Delta E_{20} = E(2^3P_2) - E(2^3P_0)$, and $\Delta E_{st} = E(2^1P_1) - E(2^3P_0)$, are tabulated for ions with nuclear charges in the range $Z=2-100$. For $Z=2$, the matrix elements are in close agreement with precise nonrelativistic variational calculations, but as Z increases from 2 to 10, the present values deviate smoothly from the variational values owing to relativistic corrections. Applications are given to determine the hyperfine structure of ^3He , $^6,7\text{Li}^+$, $^9\text{Be}^{2+}$, and $^{19}\text{F}^{7+}$. Hyperfine quenching rates of 2^3P_0 states are calculated using a radiation-damping formalism for all stable isotopes in the range $Z=6-92$. Quenching rates of 2^3P_2 states are also calculated for selected ions. For $Z=9-29$, the 2^3P_0 quenching rates are in good agreement with relativistic $1/Z$ calculations. For $Z>40$, the diagonal hyperfine matrix elements disagree in sign with previously published multiconfiguration Dirac-Fock values. In view of these differences, the present matrix elements are used to reevaluate the fine-structure intervals ΔE_{10} inferred from hyperfine quenching experiments for the ions Ni^{26+} , Ag^{45+} , and Gd^{62+} . [S1050-2947(97)06604-3]

PACS number(s): 31.30.Gs, 31.30.Jv, 31.15.Ar

I. INTRODUCTION

The hyperfine structure of 2^3P levels of heliumlike ions has been a subject of experimental and theoretical interest in atomic physics for more than thirty years. On the theoretical side, approximate methods based on product wave functions for evaluating the 2^3P hyperfine patterns were introduced by Lurio, Mandel, and Novic [1]. For neutral helium, these calculations were superseded by the variational calculations of Hambro [2], which were later extended to heliumlike ions with nuclear charges in the range $Z=2-10$ by Aashamar and Hambro [3]. In the present paper, we extend these calculations to the entire range of nuclear charges $Z=2-100$ using relativistic configuration-interaction (CI) wave functions [4,5] to evaluate the matrix elements of the magnetic-dipole hyperfine operator between substates of $2^{1,3}P$ states. In addition, we present values of the fine-structure intervals $\Delta E_{10} = E(2^3P_1) - E(2^3P_0)$, $\Delta E_{20} = E(2^3P_2) - E(2^3P_0)$, and $\Delta E_{st} = E(2^1P_1) - E(2^3P_0)$, which are needed to obtain hyperfine energy matrices for the 2^3P levels. With the data given here, accurate theoretical values of the hyperfine structure of 2^3P levels can be obtained for any ion in the range $Z=2-100$.

The hyperfine matrix elements determined here agree well with the variational calculations of Refs. [2] and [3] for $Z=2$, but disagree by a few percent with the corresponding values from Ref. [3] at $Z=10$. These differences are a consequence of the increasing importance of relativistic effects with increasing Z . Similar differences between relativistic

and nonrelativistic calculations of dipole transition amplitudes were found in Ref. [6]. We compare the present calculations with the measured hyperfine structure for ^3He [7,8], $^6,7\text{Li}^+$ [9,10], $^9\text{Be}^{2+}$ [11], and $^{19}\text{F}^{7+}$ [12]. In each of these cases, the present calculations agree with the measurements at the level of experimental accuracy. For $^6,7\text{Li}^+$, the present calculations are also in close agreement with the coupled-cluster calculations of Jette, Lee, and Das [13].

The hyperfine interaction induces small $2^{1,3}P_1$ admixtures into the 2^3P_0 wave function. Forbidden $E1$ transitions from the 2^3P_0 state to the 1^1S_0 ground state thereby become allowed, leading to a decrease in the lifetime of the 2^3P_0 state. The resulting reduction in lifetime is referred to as ‘‘hyperfine quenching.’’ The hyperfine quenching rate is sensitive to the fine-structure interval ΔE_{10} . Consequently, measurements of quenching rates can be used to infer values of ΔE_{10} , as has been shown by Indelicato *et al.* [14]. We examine the hyperfine quenching of 2^3P_0 states here, and carry out calculations of the quenched lifetimes for all stable isotopes in the range $Z=6-92$. We also examine hyperfine quenching of 2^3P_2 states and give decay rates for ions for which hyperfine quenching decreases the unperturbed lifetimes by more than 5%.

Two methods have been used in the literature to evaluate these quenching rates. For low- Z ions where the radiative level widths are small compared to the separation between levels, a perturbative method has been used. In this approach, the hyperfine structure is determined first, and radiative transitions are then calculated as perturbations. This

method was used by Mohr [15] and by Aboussaïd *et al.* [16] to evaluate 2^3P_0 quenching rates. In these low- Z calculations, it is essential to include contributions from both 2^3P_1 and 2^1P_1 states, as radiative transition amplitudes from these two states contribute *coherently* to the quenching rates. For ions with $Z > 40$ where the radiative linewidth of the 2^3P_1 level is comparable to the energy separation ΔE_{10} , the perturbative approach is no longer valid. To treat quenching for such cases, a nonperturbative approach based on the multiconfiguration Dirac-Fock (MCDF) calculation was introduced by Indelicato, Parente, and Marrus [17]. In this second approach, diagonal elements of the hyperfine energy matrix were modified to include imaginary terms arising from the radiative half-widths of the associated fine-structure levels. However, calculations carried out using this approach do not reduce precisely to perturbation theory in the limit of narrow line widths at low Z , since the coherence of the interfering 2^1P_1 and 2^3P_1 amplitudes is lost.

In the present paper, we adopt a formalism based on radiation-damping theory to treat hyperfine quenching. This formalism treats the radiation field on an equal footing with the hyperfine interaction, and is valid regardless of the size of the radiative level widths. In particular, it reduces properly to perturbation theory (including interference between transition amplitudes) when the level widths are small, and to the nonperturbative MCDF approach [17] when coherence between amplitudes is not important. In the range $Z = 9-29$, we compare the present values of 2^3P_0 quenching rates with the $1/Z$ expansion predictions of Mohr [15], and with the multiconfiguration Hartree-Fock (MCHF) calculations of Aboussaïd *et al.* [16]. For $Z > 40$, the present rates are compared with the MCDF calculations of Indelicato *et al.* [17]. Our hyperfine energy matrix elements disagree in sign and (in many cases) magnitude with values from Ref. [17]. Such differences lead to changes in predicted lifetimes ranging from 0 to 100%. In view of these differences, we reevaluate the fine-structure interval for Ni^{26+} using the experimental lifetime data obtained in Ref. [18], for Ag^{45+} using the data from Ref. [19], and for Gd^{62+} using the data from Ref. [14]. In each case, we find small differences with the original experimental determinations of ΔE_{10} .

In the following section, we set up the equations needed to evaluate the hyperfine energy shifts and quenching rates in terms of relativistic CI wave functions. In Sec. III, we present our results and compare them to other calculations and to existing experimental data.

II. THEORY

Since the 2^3P hyperfine structure is dominated by the magnetic-dipole interaction, we give the expressions needed to evaluate the hyperfine energy matrix for the 3P_J multiplet in terms of reduced matrix elements of the magnetic-dipole hyperfine operator. We have carried out calculations including the electric-quadrupole hyperfine interaction and found that the quadrupole contributions are negligible throughout the isoelectronic sequence. In the following paragraphs, we describe the evaluation of the hyperfine magnetic-dipole matrix elements using CI wave functions and determine the corresponding hyperfine energy matrix for two-electron ions.

A. Energy eigenvalue equation

We let $H = H_0 + H_{\text{hf}}$, where H_0 is the electronic Hamiltonian and H_{hf} is the hyperfine interaction operator, which is written as

$$H_{\text{hf}} = \sum_{\lambda} (-1)^{\lambda} \mathcal{M}_{-\lambda}^{(1)} \mathcal{T}_{\lambda}^{(1)}. \quad (2.1)$$

In this expression, $\mathcal{T}^{(1)}$ operates on electronic coordinates, while $\mathcal{M}^{(1)}$ operates on nuclear coordinates. We restrict our attention to four atomic states $2^3P_{0,1,2}$ and 2^1P_1 . They are designated by $|\gamma JM_J\rangle$, where $\gamma = 1$ for the singlet state and $\gamma = 3$ for the triplet states. The symbol M_J designates the magnetic quantum number of the atomic states. We expand the hyperfine state $|FM_F\rangle$ as a product of the nuclear state $|IM_I\rangle$ and atomic states $|\gamma JM_J\rangle$

$$|FM_F\rangle = \sum_{\gamma J} C_{\gamma J}^F \langle IM_I, JM_J | FM_F \rangle |IM_I\rangle |\gamma JM_J\rangle, \quad (2.2)$$

where the weight coefficients $C_{\gamma J}^F$ are to be determined. The Schrödinger equation becomes

$$\begin{aligned} (H_0 + H_{\text{hf}}) |FM_F\rangle &= \sum_{\gamma J} C_{\gamma J}^F \langle IM_I, JM_J | FM_F \rangle (E_{\gamma J} + H_{\text{hf}}) \\ &\quad \times |IM_I\rangle |\gamma JM_J\rangle \\ &= W_F |FM_F\rangle, \end{aligned} \quad (2.3)$$

where $E_{\gamma J}$ is the unperturbed energy of the state $|\gamma JM_J\rangle$. From this equation, it follows that $C_{\gamma J}^F$ satisfies the eigenvalue equation

$$W_F C_{\gamma J}^F = \sum_{\gamma' J'} W_{\gamma J, \gamma' J'}^F C_{\gamma' J'}^F, \quad (2.4)$$

where

$$\begin{aligned} W_{\gamma J, \gamma' J'}^F &= E_{\gamma J} \delta_{\gamma\gamma'} \delta_{JJ'} + (-1)^{I+J+F} \begin{Bmatrix} I & J & F \\ J' & I & 1 \end{Bmatrix} \\ &\quad \times \langle \gamma J \| \mathcal{T}^{(1)} \| \gamma' J' \rangle \langle I \| \mathcal{M}^{(1)} \| I \rangle. \end{aligned} \quad (2.5)$$

We make use of the fact that

$$\begin{aligned} \langle I \| \mathcal{M}^{(1)} \| I \rangle &= \sqrt{\frac{(2I+1)(I+1)}{I}} \langle II | \mathcal{M}_0^{(1)} | II \rangle \\ &= \sqrt{\frac{(2I+1)(I+1)}{I}} \mu_I, \end{aligned} \quad (2.6)$$

where $\mu_I = g_I I \mu_N$ is the nuclear magnetic moment, to obtain

$$\langle I \| \mathcal{M}^{(1)} \| I \rangle = \sqrt{(2I+1)I(I+1)} g_I \mu_N. \quad (2.7)$$

B. Electronic matrix elements

The CI wave function for an atomic state $|JM\rangle$ of a two-electron ion is given as

$$\Psi_{JM} = \sum_{i \leq j} c_{ij} \Phi_{ij}, \quad (2.8)$$

where the quantities c_{ij} are configuration-weight coefficients and where the configuration-state vectors Φ_{ij} are defined (in second-quantized form) by

$$\Phi_{ij} = \eta_{ij} \sum_{m_i m_j} \langle j_i m_i, j_j m_j | JM \rangle a_i^\dagger a_j^\dagger | 0 \rangle. \quad (2.9)$$

Here, η_{ij} is a normalization factor

$$\eta_{ij} = \begin{cases} 1, & i \neq j \\ 1/\sqrt{2}, & i = j. \end{cases}$$

The quantities c_{ij} , Φ_{ij} , and η_{ij} are independent of the magnetic quantum numbers m_i and m_j . Therefore, each of these quantities is characterized by the four quantum numbers $(n_i, \kappa_i, n_j, \kappa_j)$. To construct a wave function of even or odd parity, one must required the sum $l_i + l_j$ to be either even or odd, respectively. Configuration weights for the $n=2$ states of heliumlike ions, based on the relativistic no-pair Hamiltonian (including both Coulomb and Breit interactions), were obtained in Refs. [4,5] using the relativistic CI method. We use these weight coefficients in the present work. The reduced matrix element of the magnetic-dipole hyperfine operator is given by

$$\begin{aligned} \langle \gamma' J' \| \mathcal{T}^{(1)} \| \gamma J \rangle &= \sqrt{[J][J']} \sum_{\substack{m \leq n \\ r \leq s}} \eta_{rs} \eta_{mn} c_{rs}^{(\gamma' J')} c_{mn}^{(\gamma J)} \left\{ (-1)^{j_r + j_s + J + 1} \begin{Bmatrix} 1 & J & J' \\ j_s & j_r & j_m \end{Bmatrix} \langle r \| t^{(1)} \| m \rangle \delta_{ns} \right. \\ &+ (-1)^{j_r + j_n + 1} \begin{Bmatrix} 1 & J & J' \\ j_s & j_r & j_n \end{Bmatrix} \langle r \| t^{(1)} \| n \rangle \delta_{ms} + (-1)^{J' + J} \begin{Bmatrix} 1 & J & J' \\ j_r & j_s & j_m \end{Bmatrix} \langle s \| t^{(1)} \| m \rangle \delta_{nr} \\ &\left. + (-1)^{j_r + j_n + J' + 1} \begin{Bmatrix} 1 & J & J' \\ j_r & j_s & j_n \end{Bmatrix} \langle s \| t^{(1)} \| n \rangle \delta_{mr} \right\}, \quad (2.10) \end{aligned}$$

where $c_{ij}^{(\gamma' J)}$ and $c_{ij}^{(\gamma J)}$ are the weight coefficients of the initial and final states, respectively. In this equation and later, we use the notation $[J] = 2J + 1$. To derive Eq. (2.10), the operator $\mathcal{T}_\lambda^{(1)}$ is expressed in terms of the one-electron hyperfine operator $t_\lambda^{(1)}$ by

$$\mathcal{T}_\lambda^{(1)} = \sum_{ij} (t_\lambda^{(1)})_{ij} a_i^\dagger a_j. \quad (2.11)$$

The one-electron operator $t_\lambda^{(1)}$ is, in turn, given by

$$t_\lambda^{(1)}(\mathbf{r}) = -\frac{|e|}{4\pi\epsilon_0} \frac{i\sqrt{2}[\boldsymbol{\alpha} \cdot \mathbf{C}_{1\lambda}^{(0)}(\hat{\mathbf{r}})]}{cr^2}, \quad (2.12)$$

where $\mathbf{C}_{1\lambda}^{(0)}$ is a normalized magnetic vector spherical harmonic [20]. Explicit formulas for reduced matrix elements of $t_\lambda^{(1)}(\mathbf{r})$ are given in Ref. [21]. Dimensionally, the magnetic hyperfine interaction energy is given by

$$\begin{aligned} [W] &= \frac{|e|}{4\pi\epsilon_0} \frac{|e|\hbar}{2M_p} \frac{1}{ca_0^2} = \frac{1}{2M_p c} \text{ a.u.} = 1.987131 \times 10^{-6} \text{ a.u.} \\ &= 0.4361249 \text{ cm}^{-1} = 13074.70 \text{ MHz.} \end{aligned}$$

In the following, we express the nuclear magnetic moment in units of μ_N and evaluate $t_\lambda^{(1)}(\mathbf{r})$ in atomic units. The resulting hyperfine energies will then be in the units above.

Using the expansion coefficients from the relativistic CI calculations of Refs. [4,5] in the above formulas,

one readily obtains the dipole matrix elements. In Table I, we present the CI values of the four reduced matrix elements $\langle \gamma' J' \| \mathcal{T}^{(1)} \| \gamma J \rangle \equiv \langle 31 \| \mathcal{T}^{(1)} \| 30 \rangle$, $\langle 31 \| \mathcal{T}^{(1)} \| 31 \rangle$, $\langle 31 \| \mathcal{T}^{(1)} \| 32 \rangle$, and $\langle 32 \| \mathcal{T}^{(1)} \| 32 \rangle$ for heliumlike ions with $Z=2-100$. The matrix elements $\langle 31 \| \mathcal{T}^{(1)} \| 32 \rangle$ are particularly sensitive to the Breit interaction and change by as much as a factor of 2 over the range considered when the Breit interaction is omitted from the CI wave function. In Table II, we present values of the four matrix elements $\langle 11 \| \mathcal{T}^{(1)} \| 30 \rangle$, $\langle 11 \| \mathcal{T}^{(1)} \| 31 \rangle$, $\langle 11 \| \mathcal{T}^{(1)} \| 32 \rangle$, and $\langle 11 \| \mathcal{T}^{(1)} \| 11 \rangle$, also in the range $Z=2-100$. Finally, the three fine-structure intervals ΔE_{10} , ΔE_{20} , and ΔE_{st} are presented in Table III. For $Z=2$ and 3, the values of ΔE_{10} and ΔE_{20} are taken from Refs. [7] and [9], respectively, while for $Z=2-6$, the values of ΔE_{st} are from Drake [22]. Remaining values of the three intervals are from relativistic CI calculations that include QED and mass-polarization corrections. These energies were compared with other precise calculations and with experiment in Refs. [4,5]. Similar comparisons for the matrix elements will be given in Sec. III A.

C. Radiative decay of hyperfine levels

As mentioned in the Introduction, two approaches have been used to treat the radiative decay of hyperfine levels. The first of these is the perturbative approach used in Refs. [15] and [16] in which the hyperfine levels are first determined by diagonalizing the hyperfine energy matrix, and the radiation field is then considered as a perturbation that induces transitions between the hyperfine levels and lower-energy states.

TABLE I. Reduced matrix elements $\langle \gamma J \| T^{(1)} \| \gamma' J' \rangle$ of the dipole hyperfine operator between 2^3P_J states ($\gamma=3$) for heliumlike ions. Numbers in brackets represent powers of 10.

Z	$\langle 31 \ T^{(1)} \ 30 \rangle$	$\langle 31 \ T^{(1)} \ 31 \rangle$	$\langle 31 \ T^{(1)} \ 32 \rangle$	$\langle 32 \ T^{(1)} \ 32 \rangle$	Z	$\langle 31 \ T^{(1)} \ 30 \rangle$	$\langle 31 \ T^{(1)} \ 31 \rangle$	$\langle 31 \ T^{(1)} \ 32 \rangle$	$\langle 32 \ T^{(1)} \ 32 \rangle$
2	1.0780[-1]	9.5594[-2]	1.2118[-1]	2.1191[-1]	53	3.0080[3]	4.6353[3]	1.7712[2]	5.0784[3]
3	3.5906[-1]	3.2659[-1]	4.0583[-1]	7.1702[-1]	54	3.2111[3]	4.9513[3]	1.7407[2]	5.4209[3]
4	8.4749[-1]	7.8338[-1]	9.5962[-1]	1.7074[0]	55	3.4266[3]	5.2866[3]	1.7092[2]	5.7844[3]
5	1.6539[0]	1.5472[0]	1.8712[0]	3.3485[0]	56	3.6528[3]	5.6389[3]	1.6752[2]	6.1661[3]
6	2.8606[0]	2.7045[0]	3.2263[0]	5.8064[0]	57	3.8914[3]	6.0106[3]	1.6396[2]	6.5688[3]
7	4.5528[0]	4.3496[0]	5.1068[0]	9.2486[0]	58	4.1426[3]	6.4023[3]	1.6019[2]	6.9929[3]
8	6.8187[0]	6.5876[0]	7.5885[0]	1.3844[1]	59	4.4073[3]	6.8151[3]	1.5624[2]	7.4398[3]
9	9.7513[0]	9.5384[0]	1.0739[1]	1.9762[1]	60	4.6859[3]	7.2499[3]	1.5228[2]	7.9102[3]
10	1.3449[1]	1.3340[1]	1.4615[1]	2.7176[1]	61	4.9784[3]	7.7067[3]	1.4790[2]	8.4043[3]
11	1.8019[1]	1.8154[1]	1.9262[1]	3.6263[1]	62	5.2853[3]	8.1866[3]	1.4329[2]	8.9230[3]
12	2.3572[1]	2.4164[1]	2.4703[1]	4.7197[1]	63	5.6104[3]	8.6950[3]	1.3854[2]	9.4723[3]
13	3.0230[1]	3.1586[1]	3.0949[1]	6.0162[1]	64	5.9495[3]	9.2261[3]	1.3349[2]	1.0046[4]
14	3.8121[1]	4.0662[1]	3.7983[1]	7.5336[1]	65	6.3109[3]	9.7919[3]	1.2835[2]	1.0657[4]
15	4.7383[1]	5.1665[1]	4.5764[1]	9.2908[1]	66	6.6894[3]	1.0385[4]	1.2295[2]	1.1297[4]
16	5.8161[1]	6.4900[1]	5.4228[1]	1.1307[2]	67	7.0833[3]	1.1004[4]	1.1721[2]	1.1964[4]
17	7.0606[1]	8.0687[1]	6.3283[1]	1.3601[2]	68	7.5061[3]	1.1668[4]	1.1144[2]	1.2679[4]
18	8.4872[1]	9.9367[1]	7.2814[1]	1.6193[2]	69	7.9461[3]	1.2359[4]	1.0532[2]	1.3424[4]
19	1.0113[2]	1.2130[2]	8.2692[1]	1.9105[2]	70	8.4041[3]	1.3081[4]	9.8857[1]	1.4200[4]
20	1.1952[2]	1.4680[2]	9.2753[1]	2.2355[2]	71	8.8966[3]	1.3856[4]	9.2335[1]	1.5033[4]
21	1.4020[2]	1.7621[2]	1.0285[2]	2.5966[2]	72	9.4027[3]	1.4656[4]	8.5345[1]	1.5892[4]
22	1.6332[2]	2.0982[2]	1.1281[2]	2.9960[2]	73	9.9492[3]	1.5517[4]	7.8309[1]	1.6818[4]
23	1.8904[2]	2.4791[2]	1.2251[2]	3.4361[2]	74	1.0507[4]	1.6400[4]	7.0732[1]	1.7764[4]
24	2.1749[2]	2.9071[2]	1.3180[2]	3.9190[2]	75	1.1115[4]	1.7362[4]	6.3170[1]	1.8795[4]
25	2.4877[2]	3.3839[2]	1.4055[2]	4.4469[2]	76	1.1736[4]	1.8348[4]	5.5057[1]	1.9850[4]
26	2.8307[2]	3.9117[2]	1.4871[2]	5.0227[2]	77	1.2408[4]	1.9412[4]	4.6842[1]	2.0990[4]
27	3.2048[2]	4.4917[2]	1.5620[2]	5.6488[2]	78	1.3096[4]	2.0507[4]	3.8107[1]	2.2160[4]
28	3.6120[2]	5.1261[2]	1.6302[2]	6.3286[2]	79	1.3843[4]	2.1695[4]	2.9259[1]	2.3429[4]
29	4.0520[2]	5.8144[2]	1.6908[2]	7.0621[2]	80	1.4600[4]	2.2905[4]	1.9796[1]	2.4720[4]
30	4.5279[2]	6.5602[2]	1.7446[2]	7.8550[2]	81	1.5434[4]	2.4233[4]	1.0280[1]	2.6137[4]
31	5.0406[2]	7.3639[2]	1.7915[2]	8.7094[2]	82	1.6277[4]	2.5585[4]	1.2209[-1]	2.7575[4]
32	5.5917[2]	8.2285[2]	1.8319[2]	9.6277[2]	83	1.7201[4]	2.7062[4]	-1.0174[1]	2.9147[4]
33	6.1834[2]	9.1566[2]	1.8664[2]	1.0614[3]	84	1.8139[4]	2.8572[4]	-2.1091[1]	3.0750[4]
34	6.8166[2]	1.0149[3]	1.8951[2]	1.1671[3]	85	1.9165[4]	3.0218[4]	-3.2219[1]	3.2499[4]
35	7.4950[2]	1.1211[3]	1.9188[2]	1.2804[3]	86	2.0189[4]	3.1876[4]	-4.4062[1]	3.4254[4]
36	8.2179[2]	1.2342[3]	1.9373[2]	1.4012[3]	87	2.1345[4]	3.3736[4]	-5.6009[1]	3.6226[4]
37	8.9899[2]	1.3549[3]	1.9516[2]	1.5304[3]	88	2.2494[4]	3.5601[4]	-6.8791[1]	3.8196[4]
38	9.8128[2]	1.4833[3]	1.9618[2]	1.6681[3]	89	2.3787[4]	3.7690[4]	-8.1704[1]	4.0406[4]
39	1.0688[3]	1.6199[3]	1.9683[2]	1.8149[3]	90	2.5020[4]	3.9713[4]	-9.5587[1]	4.2533[4]
40	1.1619[3]	1.7648[3]	1.9711[2]	1.9708[3]	91	2.6511[4]	4.2125[4]	-1.0934[2]	4.5080[4]
41	1.2606[3]	1.9186[3]	1.9706[2]	2.1365[3]	92	2.7914[4]	4.4433[4]	-1.2419[2]	4.7502[4]
42	1.3652[3]	2.0814[3]	1.9668[2]	2.3121[3]	93	2.9546[4]	4.7093[4]	-1.3921[2]	5.0302[4]
43	1.4765[3]	2.2544[3]	1.9608[2]	2.4991[3]	94	3.1107[4]	4.9679[4]	-1.5520[2]	5.3005[4]
44	1.5941[3]	2.4373[3]	1.9517[2]	2.6968[3]	95	3.2940[4]	5.2683[4]	-1.7146[2]	5.6158[4]
45	1.7188[3]	2.6311[3]	1.9403[2]	2.9065[3]	96	3.4698[4]	5.5612[4]	-1.8869[2]	5.9210[4]
46	1.8507[3]	2.8362[3]	1.9266[2]	3.1285[3]	97	3.6754[4]	5.9002[4]	-2.0630[2]	6.2757[4]
47	1.9904[3]	3.0532[3]	1.9108[2]	3.3635[3]	98	3.8718[4]	6.2301[4]	-2.2489[2]	6.6180[4]
48	2.1375[3]	3.2819[3]	1.8923[2]	3.6114[3]	99	4.1011[4]	6.6110[4]	-2.4399[2]	7.0150[4]
49	2.2936[3]	3.5244[3]	1.8722[2]	3.8741[3]	100	4.3212[4]	6.9840[4]	-2.6405[2]	7.4004[4]
50	2.4580[3]	3.7800[3]	1.8499[2]	4.1512[3]					
51	2.6315[3]	4.0496[3]	1.8255[2]	4.4436[3]					
52	2.8138[3]	4.3333[3]	1.7986[2]	4.7510[3]					

TABLE II. Reduced matrix elements $\langle \gamma J \| T^{(1)} \| \gamma' J' \rangle$ of the dipole hyperfine operator between substates of the 2^1P_1 state ($\gamma=1$) and 2^3P_J states ($\gamma=3$) for heliumlike ions. Numbers in brackets represent powers of 10.

Z	$\langle 11 \ T^{(1)} \ 30 \rangle$	$\langle 11 \ T^{(1)} \ 31 \rangle$	$\langle 11 \ T^{(1)} \ 32 \rangle$	$\langle 11 \ T^{(1)} \ 11 \rangle$	Z	$\langle 11 \ T^{(1)} \ 30 \rangle$	$\langle 11 \ T^{(1)} \ 31 \rangle$	$\langle 11 \ T^{(1)} \ 32 \rangle$	$\langle 11 \ T^{(1)} \ 11 \rangle$
2	-7.6578[-2]	-1.3371[-1]	1.7214[-1]	6.0871[-4]	52	-1.4851[2]	-3.0260[2]	4.6255[3]	-2.0024[3]
3	-2.5691[-1]	-4.5289[-1]	5.8134[-1]	4.8478[-3]	53	-1.4923[2]	-3.0239[2]	4.9457[3]	-2.1431[3]
4	-6.0721[-1]	-1.0777[0]	1.3818[0]	1.5366[-2]	54	-1.4987[2]	-3.0192[2]	5.2807[3]	-2.2902[3]
5	-1.1828[0]	-2.1101[0]	2.7069[0]	3.2101[-2]	55	-1.5056[2]	-3.0147[2]	5.6363[3]	-2.4463[3]
6	-2.0372[0]	-3.6508[0]	4.6926[0]	5.0184[-2]	56	-1.5122[2]	-3.0084[2]	6.0097[3]	-2.6102[3]
7	-3.2218[0]	-5.7987[0]	7.4793[0]	5.7483[-2]	57	-1.5189[2]	-3.0014[2]	6.4039[3]	-2.7832[3]
8	-4.7841[0]	-8.6490[0]	1.1213[1]	3.1530[-2]	58	-1.5255[2]	-2.9935[2]	6.8190[3]	-2.9654[3]
9	-6.7666[0]	-1.2292[1]	1.6046[1]	-6.3806[-2]	59	-1.5323[2]	-2.9848[2]	7.2566[3]	-3.1574[3]
10	-9.2057[0]	-1.6813[1]	2.2141[1]	-2.8219[-1]	60	-1.5392[2]	-2.9752[2]	7.7173[3]	-3.3596[3]
11	-1.2130[1]	-2.2286[1]	2.9674[1]	-6.9700[-1]	61	-1.5460[2]	-2.9643[2]	8.2013[3]	-3.5720[3]
12	-1.5556[1]	-2.8770[1]	3.8824[1]	-1.4081[0]	62	-1.5527[2]	-2.9523[2]	8.7095[3]	-3.7950[3]
13	-1.9492[1]	-3.6312[1]	4.9796[1]	-2.5406[0]	63	-1.5601[2]	-2.9405[2]	9.2480[3]	-4.0314[3]
14	-2.3927[1]	-4.4932[1]	6.2794[1]	-4.2483[0]	64	-1.5670[2]	-2.9265[2]	9.8101[3]	-4.2781[3]
15	-2.8841[1]	-5.4626[1]	7.8046[1]	-6.7131[0]	65	-1.5750[2]	-2.9137[2]	1.0409[4]	-4.5412[3]
16	-3.4195[1]	-6.5362[1]	9.5790[1]	-1.0143[1]	66	-1.5829[2]	-2.8994[2]	1.1037[4]	-4.8169[3]
17	-3.9934[1]	-7.7066[1]	1.1627[2]	-1.4767[1]	67	-1.5903[2]	-2.8829[2]	1.1691[4]	-5.1042[3]
18	-4.5991[1]	-8.9632[1]	1.3973[2]	-2.0827[1]	68	-1.5993[2]	-2.8682[2]	1.2394[4]	-5.4127[3]
19	-5.2288[1]	-1.0293[2]	1.6646[2]	-2.8571[1]	69	-1.6078[2]	-2.8512[2]	1.3125[4]	-5.7341[3]
20	-5.8729[1]	-1.1675[2]	1.9668[2]	-3.8233[1]	70	-1.6158[2]	-2.8321[2]	1.3887[4]	-6.0691[3]
21	-6.5220[1]	-1.3092[2]	2.3065[2]	-5.0035[1]	71	-1.6257[2]	-2.8149[2]	1.4706[4]	-6.4293[3]
22	-7.1669[1]	-1.4521[2]	2.6863[2]	-6.4167[1]	72	-1.6342[2]	-2.7938[2]	1.5550[4]	-6.8002[3]
23	-7.7988[1]	-1.5941[2]	3.1085[2]	-8.0789[1]	73	-1.6447[2]	-2.7751[2]	1.6460[4]	-7.2007[3]
24	-8.4096[1]	-1.7330[2]	3.5754[2]	-1.0002[2]	74	-1.6536[2]	-2.7516[2]	1.7391[4]	-7.6099[3]
25	-8.9917[1]	-1.8667[2]	4.0887[2]	-1.2192[2]	75	-1.6650[2]	-2.7316[2]	1.8406[4]	-8.0569[3]
26	-9.5415[1]	-1.9939[2]	4.6513[2]	-1.4656[2]	76	-1.6748[2]	-2.7068[2]	1.9444[4]	-8.5138[3]
27	-1.0055[2]	-2.1133[2]	5.2649[2]	-1.7397[2]	77	-1.6866[2]	-2.6841[2]	2.0566[4]	-9.0079[3]
28	-1.0531[2]	-2.2244[2]	5.9327[2]	-2.0420[2]	78	-1.6972[2]	-2.6571[2]	2.1718[4]	-9.5156[3]
29	-1.0966[2]	-2.3257[2]	6.6542[2]	-2.3715[2]	79	-1.7099[2]	-2.6325[2]	2.2969[4]	-1.0067[4]
30	-1.1364[2]	-2.4183[2]	7.4346[2]	-2.7295[2]	80	-1.7208[2]	-2.6024[2]	2.4240[4]	-1.0627[4]
31	-1.1735[2]	-2.5035[2]	8.2754[2]	-3.1152[2]	81	-1.7345[2]	-2.5758[2]	2.5638[4]	-1.1243[4]
32	-1.2062[2]	-2.5782[2]	9.1790[2]	-3.5304[2]	82	-1.7463[2]	-2.5435[2]	2.7055[4]	-1.1868[4]
33	-1.2357[2]	-2.6449[2]	1.0150[3]	-3.9756[2]	83	-1.7605[2]	-2.5138[2]	2.8607[4]	-1.2553[4]
34	-1.2623[2]	-2.7037[2]	1.1188[3]	-4.4507[2]	84	-1.7733[2]	-2.4789[2]	3.0188[4]	-1.3251[4]
35	-1.2864[2]	-2.7559[2]	1.2301[3]	-4.9580[2]	85	-1.7882[2]	-2.4460[2]	3.1915[4]	-1.4014[4]
36	-1.3079[2]	-2.8012[2]	1.3487[3]	-5.4969[2]	86	-1.8011[2]	-2.4064[2]	3.3647[4]	-1.4778[4]
37	-1.3274[2]	-2.8410[2]	1.4754[3]	-6.0704[2]	87	-1.8173[2]	-2.3712[2]	3.5596[4]	-1.5640[4]
38	-1.3450[2]	-2.8757[2]	1.6105[3]	-6.6795[2]	88	-1.8314[2]	-2.3294[2]	3.7542[4]	-1.6499[4]
39	-1.3611[2]	-2.9056[2]	1.7542[3]	-7.3256[2]	89	-1.8484[2]	-2.2905[2]	3.9727[4]	-1.7466[4]
40	-1.3755[2]	-2.9312[2]	1.9070[3]	-8.0100[2]	90	-1.8621[2]	-2.2423[2]	4.1829[4]	-1.8394[4]
41	-1.3887[2]	-2.9528[2]	2.0692[3]	-8.7346[2]	91	-1.8812[2]	-2.2010[2]	4.4350[4]	-1.9511[4]
42	-1.4005[2]	-2.9706[2]	2.2410[3]	-9.5002[2]	92	-1.8966[2]	-2.1501[2]	4.6745[4]	-2.0570[4]
43	-1.4117[2]	-2.9862[2]	2.4239[3]	-1.0313[3]	93	-1.9157[2]	-2.1023[2]	4.9517[4]	-2.1798[4]
44	-1.4219[2]	-2.9984[2]	2.6172[3]	-1.1171[3]	94	-1.9320[2]	-2.0466[2]	5.2192[4]	-2.2981[4]
45	-1.4314[2]	-3.0085[2]	2.8222[3]	-1.2079[3]	95	-1.9520[2]	-1.9933[2]	5.5316[4]	-2.4365[4]
46	-1.4404[2]	-3.0164[2]	3.0393[3]	-1.3039[3]	96	-1.9695[2]	-1.9329[2]	5.8338[4]	-2.5704[4]
47	-1.4489[2]	-3.0224[2]	3.2691[3]	-1.4053[3]	97	-1.9904[2]	-1.8732[2]	6.1855[4]	-2.7263[4]
48	-1.4566[2]	-3.0260[2]	3.5113[3]	-1.5121[3]	98	-2.0089[2]	-1.8069[2]	6.5247[4]	-2.8766[4]
49	-1.4644[2]	-3.0287[2]	3.7682[3]	-1.6253[3]	99	-2.0305[2]	-1.7400[2]	6.9184[4]	-3.0513[4]
50	-1.4717[2]	-3.0295[2]	4.0391[3]	-1.7445[3]	100	-2.0503[2]	-1.6674[2]	7.3005[4]	-3.2207[4]
51	-1.4786[2]	-3.0287[2]	4.3249[3]	-1.8702[3]					

TABLE III. Energy intervals $\Delta E_{10}=E(2^3P_1)-E(2^3P_0)$, $\Delta E_{20}=E(2^3P_2)-E(2^3P_0)$, and $\Delta E_{st}=E(2^1P_1)-E(2^3P_0)$ in a.u. from the CI calculations of Ref. [4,5], including QED and mass polarization corrections. Numbers in brackets represent powers of 10.

Z	ΔE_{10}	ΔE_{20}	ΔE_{st}	Z	ΔE_{10}	ΔE_{20}	ΔE_{st}
2	-4.5013[-6]	-4.8495[-6]	9.3284[-3]	52	-1.5466[-1]	1.1930[1]	1.3188[1]
3	-2.3663[-5]	-1.4137[-5]	3.4367[-2]	53	-1.8567[-1]	1.2952[1]	1.4238[1]
4	-5.2600[-5]	1.5000[-5]	6.4196[-2]	54	-2.1880[-1]	1.4042[1]	1.5356[1]
5	-7.3900[-5]	1.6620[-4]	9.5874[-2]	55	-2.5413[-1]	1.5203[1]	1.6545[1]
6	-5.6900[-5]	5.6190[-4]	1.2854[-1]	56	-2.9171[-1]	1.6439[1]	1.7810[1]
7	3.9800[-5]	1.3657[-3]	1.6186[-1]	57	-3.3161[-1]	1.7752[1]	1.9153[1]
8	2.6780[-4]	2.7812[-3]	1.9581[-1]	58	-3.7391[-1]	1.9148[1]	2.0578[1]
9	6.8930[-4]	5.0538[-3]	2.3042[-1]	59	-4.1870[-1]	2.0629[1]	2.2089[1]
10	1.3700[-3]	8.4690[-3]	2.6588[-1]	60	-4.6604[-1]	2.2201[1]	2.3691[1]
11	2.3830[-3]	1.3351[-2]	3.0231[-1]	61	-5.1600[-1]	2.3865[1]	2.5388[1]
12	3.7960[-3]	2.0072[-2]	3.4003[-1]	62	-5.6867[-1]	2.5628[1]	2.7183[1]
13	5.6820[-3]	2.9041[-2]	3.7928[-1]	63	-6.2413[-1]	2.7497[1]	2.9082[1]
14	8.0940[-3]	4.0707[-2]	4.2046[-1]	64	-6.8249[-1]	2.9473[1]	3.1090[1]
15	1.1082[-2]	5.5569[-2]	4.6394[-1]	65	-7.4384[-1]	3.1562[1]	3.3211[1]
16	1.4674[-2]	7.4167[-2]	5.1026[-1]	66	-8.0828[-1]	3.3768[1]	3.5451[1]
17	1.8884[-2]	9.7083[-2]	5.5990[-1]	67	-8.7589[-1]	3.6099[1]	3.7815[1]
18	2.3692[-2]	1.2494[-1]	6.1346[-1]	68	-9.4680[-1]	3.8558[1]	4.0308[1]
19	2.9063[-2]	1.5842[-1]	6.7176[-1]	69	-1.0211[0]	4.1153[1]	4.2937[1]
20	3.4928[-2]	1.9823[-1]	7.3545[-1]	70	-1.0990[0]	4.3888[1]	4.5708[1]
21	4.1193[-2]	2.4514[-1]	8.0531[-1]	71	-1.1805[0]	4.6772[1]	4.8627[1]
22	4.7746[-2]	2.9997[-1]	8.8227[-1]	72	-1.2657[0]	4.9809[1]	5.1700[1]
23	5.4461[-2]	3.6357[-1]	9.6736[-1]	73	-1.3549[0]	5.3008[1]	5.4936[1]
24	6.1195[-2]	4.3685[-1]	1.0616[0]	74	-1.4481[0]	5.6375[1]	5.8340[1]
25	6.7795[-2]	5.2078[-1]	1.1660[0]	75	-1.5455[0]	5.9919[1]	6.1921[1]
26	7.4119[-2]	6.1636[-1]	1.2817[0]	76	-1.6473[0]	6.3646[1]	6.5686[1]
27	8.0025[-2]	7.2466[-1]	1.4099[0]	77	-1.7536[0]	6.7566[1]	6.9645[1]
28	8.5379[-2]	8.4680[-1]	1.5519[0]	78	-1.8645[0]	7.1686[1]	7.3804[1]
29	9.0053[-2]	9.8396[-1]	1.7088[0]	79	-1.9803[0]	7.6017[1]	7.8175[1]
30	9.3930[-2]	1.1374[0]	1.8820[0]	80	-2.1011[0]	8.0567[1]	8.2765[1]
31	9.6904[-2]	1.3083[0]	2.0729[0]	81	-2.2271[0]	8.5346[1]	8.7585[1]
32	9.8890[-2]	1.4981[0]	2.2828[0]	82	-2.3586[0]	9.0366[1]	9.2647[1]
33	9.9815[-2]	1.7081[0]	2.5132[0]	83	-2.4957[0]	9.5636[1]	9.7959[1]
34	9.9610[-2]	1.9399[0]	2.7657[0]	84	-2.6388[0]	1.0117[2]	1.0353[2]
35	9.8216[-2]	2.1950[0]	3.0418[0]	85	-2.7880[0]	1.0698[2]	1.0938[2]
36	9.5570[-2]	2.4750[0]	3.3430[0]	86	-2.9436[0]	1.1307[2]	1.1552[2]
37	9.1615[-2]	2.7815[0]	3.6711[0]	87	-3.1058[0]	1.1946[2]	1.2196[2]
38	8.6310[-2]	3.1162[0]	4.0279[0]	88	-3.2748[0]	1.2617[2]	1.2872[2]
39	7.9615[-2]	3.4811[0]	4.4151[0]	89	-3.4509[0]	1.3321[2]	1.3580[2]
40	7.1480[-2]	3.8779[0]	4.8346[0]	90	-3.6346[0]	1.4060[2]	1.4323[2]
41	6.1855[-2]	4.3086[0]	5.2884[0]	91	-3.8263[0]	1.4834[2]	1.5102[2]
42	5.0700[-2]	4.7753[0]	5.7785[0]	92	-4.0262[0]	1.5647[2]	1.5920[2]
43	3.7972[-2]	5.2801[0]	6.3071[0]	93	-4.2347[0]	1.6499[2]	1.6777[2]
44	2.3640[-2]	5.8251[0]	6.8763[0]	94	-4.4521[0]	1.7393[2]	1.7675[2]
45	7.6657[-3]	6.4128[0]	7.4885[0]	95	-4.6789[0]	1.8330[2]	1.8618[2]
46	-1.0010[-2]	7.0453[0]	8.1461[0]	96	-4.9157[0]	1.9314[2]	1.9606[2]
47	-2.9450[-2]	7.7253[0]	8.8514[0]	97	-5.1630[0]	2.0346[2]	2.0643[2]
48	-5.0720[-2]	8.4553[0]	9.6070[0]	98	-5.4213[0]	2.1428[2]	2.1731[2]
49	-7.3813[-2]	9.2379[0]	1.0416[1]	99	-5.6907[0]	2.2564[2]	2.2872[2]
50	-9.8780[-2]	1.0076[1]	1.1280[1]	100	-5.9709[0]	2.3756[2]	2.4069[2]
51	-1.2571[-1]	1.0972[1]	1.2204[1]				

This approach is appropriate for cases such as the decay of 2^3P_0 states in low- Z ions where radiative linewidths of the fine-structure levels are small compared to the level spacings. A second approach, used in Ref. [17], is a nonperturbative approach in which the radiation field and the hyperfine interaction are treated on the same footing. Such an approach is needed to describe hyperfine quenching in the range $Z > 40$, where the radiative linewidth of the 2^3P_1 state becomes comparable to the energy separation ΔE_{10} . In Ref. [17], the hyperfine energy matrix was modified to include effects of the radiation field by adding the radiative half-widths of the fine-structure levels as imaginary parts to the diagonal matrix elements. The modified hyperfine energy eigenvalue equation was then solved. The real parts of the energy eigenvalues gave the level shifts and the imaginary parts gave the hyperfine level half-widths, from which quenching rates were determined.

In cases where the radiative half-widths of the fine-structure levels are small compared to the fine-structure spacing, the second method reduces to the first, provided interferences between transitions from different sublevels are ignored. In perturbation theory, such interferences occur between transition amplitudes from the 2^3P_1 and 2^1P_1 states. Even though the 2^1P_1 state is only weakly coupled to the 2^3P_J states by the hyperfine interaction, these interferences can be very important, as the amplitude of the transition

$2^1P_1 \rightarrow 1^1S_0$ is much larger than the corresponding $2^3P_1 \rightarrow 1^1S_0$ amplitude for low- Z ions. These amplitudes interfere (constructively) to give a rate that is substantially larger than the weighted sum of the rates from the two individual levels. For $Z > 40$, the contribution of the 2^1P_1 state to the decay rate of the 2^3P_0 levels decreases to less than 1%, so neglecting interferences is not expected to give large errors.

Here, we adopt a method based on radiation-damping theory to treat both wide and narrow levels. This theory leads again to a complex generalization of the hyperfine energy matrix, with imaginary diagonal contributions corresponding to radiative half-widths. Additionally, however, radiation-damping theory gives imaginary contributions to the off-diagonal 2^3P_1 - 2^1P_1 matrix element. Decay rates calculated using radiation-damping theory reduce precisely to the results of perturbation theory, including coherence effects, in the limit of small level widths.

1. Perturbative approach

Let us consider the amplitude for an electromagnetic multipole transition from hyperfine component F of a 2^3P_J state to hyperfine component F' of a lower 2^3S_1 or 1^1S_0 state. Using the notation of Ref. [6], we may write this transition amplitude as

$$\langle (n\gamma' S_{J'} I) F' \| Q_k^{(\lambda)} \| (2\gamma P_J I) F \rangle = \sum_{\gamma} \sqrt{[F][F']} (-1)^{J+k+F'+I} \begin{Bmatrix} F' & F & k \\ J & J' & I \end{Bmatrix} \sum_{\gamma} C_{\gamma J}^F \langle n\gamma' S_{J'} \| Q_k^{(\lambda)} \| 2\gamma P_J \rangle, \quad (2.13)$$

where $Q_{kq}^{(\lambda)}$ is the electromagnetic multipole operator of order k . The superscript λ designates the type of multipole: $\lambda = 1$ for electric multipoles and $\lambda = 0$ for magnetic multipoles. The angular coefficients of the contributions from the 2^3P_1 and 2^1P_1 states to the sum in the above equation are identical. It follows that these two contributions to the decay rate add coherently. For electric dipole transitions, the line strength of the transition from F to F' is

$$S(F', F) = |\langle (n\gamma' S_{J'} I) F' \| Q_1 \| (2\gamma P_J I) F \rangle|^2,$$

where $Q_1 \equiv Q_1^{(1)}$. For decays of 2^3P_J states, there are three channels to consider:

a. $2^3P_J \rightarrow 1^1S_0(E1)$: In this case, $F' = I$ and there are contributions to the decay of the 2^3P_J state from initial substates distributed over the various possible hyperfine components F . We average over the $[I] \times [J]$ initial substates to find

$$A_{E1} = \frac{2.02613 \times 10^{18}}{\lambda^3} \sum_F \frac{S_{E1}(I, F)}{[I][J]} = \frac{2.02613 \times 10^{18}}{\lambda^3} \sum_F \frac{[F]}{3[I][J]} \left| \sum_{\gamma} C_{\gamma 1}^F \langle 1^1S_0 \| Q_1 \| 2\gamma P_1 \rangle \right|^2, \quad (2.14)$$

where A_{E1} is the decay rate in s^{-1} , S_{E1} is the line strength in a.u., and λ is the wavelength in Å for the $2^3P_J \rightarrow 1^1S_0$ transition. (Small differences in λ between hyperfine components are ignored here.) To evaluate this expression, it is necessary to know the unperturbed reduced matrix elements $\langle 1^1S_0 \| Q_1 \| 2^1P_1 \rangle$ and $\langle 1^1S_0 \| Q_1 \| 2^3P_1 \rangle$. These can be obtained as square roots of the line strengths tabulated in Ref. [6]. To be consistent with the phase conventions chosen here for the magnetic-dipole hyperfine matrix elements, the relative signs of these two reduced matrix elements must be negative.

b. $2^3P_J \rightarrow 2^3S_1(E1)$: In this case, we find

$$A'_{E1} = \frac{2.02613 \times 10^{18}}{\lambda^3} \sum_{F'F} \frac{S'_{E1}(F', F)}{[I][J]} = \frac{2.02613 \times 10^{18}}{\lambda^3} \left\{ \sum_F \frac{[F]}{[I][J]} |C_{30}^F|^2 \times |\langle 2^3S_1 \| Q_1 \| 2^3P_0 \rangle|^2 \right. \\ \left. + \sum_F \frac{[F]}{3[I][J]} \left| \sum_{\gamma} C_{\gamma 1}^F \langle 2^3S_1 \| Q_1 \| 2\gamma P_1 \rangle \right|^2 + \sum_F \frac{[F]}{5[I][J]} |C_{32}^F|^2 \times |\langle 2^3S_1 \| Q_1 \| 2^3P_2 \rangle|^2 \right\}, \quad (2.15)$$

where λ is the wavelength of the $2^3P_J \rightarrow 2^3S_1$ transition. Again, the reduced matrix elements $\langle 2^3S_1 \| Q_1 \| 2^1P_1 \rangle$ and $\langle 2^3S_1 \| Q_1 \| 2^3P_1 \rangle$ can be obtained as square roots of the associated line strengths tabulated in Ref. [6], but in this case with a positive relative sign.

c. $2^3P_J \rightarrow 1^1S_0(M2)$: In this case, we may write

$$A_{M2} = \frac{1.49097 \times 10^{13}}{\lambda^5} \sum_F \frac{S_{M2}(I, F)}{[I][J]} = \frac{1.49097 \times 10^{13}}{\lambda^5} \sum_F \frac{[F]}{5[I][J]} |C_{32}^F|^2 \times |\langle 1^1S_0 \| M_2 \| 2^3P_2 \rangle|^2. \quad (2.16)$$

Here, $M_2 = 2cQ_2^{(0)}$ is the magnetic-quadrupole moment operator, and λ is the wavelength of the $2^3P_J \rightarrow 1^1S_0$ transition. Since only one component of each hyperfine level contributes to the decay in this case, there is no question of coherence.

For the 2^3P_0 state, there is only one hyperfine component $F=I$, so the sums on the right-hand sides of the above equations collapse to a single term. The $M2$ contributions are included in our calculations of the 2^3P_0 decay rate, but prove to be negligible as the coupling between the 2^3P_0 and 2^3P_2 states are very weak. For the decay of the 2^3P_2 state, all values of F in the range $|I-2| \leq F \leq I+2$ are included, and the $M2$ contributions to the decay rate are substantial for high- Z ions.

2. Radiation-damping method

For cases where the radiative linewidth is comparable to the separation between levels, the perturbative approach described above is inadequate. In such cases, the interaction with the radiation field must be treated on an equal footing with the hyperfine interaction. One particularly convenient method for including radiative corrections in atomic wave functions is by means of the nonlocal, optical potential V_{rd} introduced by Robicheaux *et al.* [23] to treat radiation damping. If we let $Q_{kq}^{(\lambda)}$ represent the electromagnetic multipole operator, then V_{rd} is defined by its action on a state $|\psi_E\rangle$ of energy E by

$$V_{\text{rd}}|\psi_E\rangle = i\alpha \sum_{kq\lambda} \frac{(k+1)(2k+1)}{k[(2k+1)!!]^2} \sum_n (E-E_n) \times k_n^{2J} Q_{kq}^{(\lambda)} |\psi_n\rangle \langle \psi_n | Q_{kq}^{(\lambda)\dagger} | \psi_E \rangle, \quad (2.17)$$

where α is the fine-structure constant and $k_n = (E-E_n)/\hbar c$ is the wave number of the photon connecting states ψ_E and ψ_n . The sum over n ranges over all states having energy less than E . For the 2^3P_J states considered here, only two states n contribute, the 1^1S_0 ground state and the 2^3S_1 state.

The potential V_{rd} is a spherically symmetric, anti-Hermitian operator, and its matrix elements are nonvanishing

only between states that have the same angular momentum. Therefore, for $2^1, 3P_J$ states, there are four diagonal matrix elements and only one nonvanishing off-diagonal matrix element. These matrix elements are given by (in a.u.)

$$\langle 2^3P_0 | V_{\text{rd}} | 2^3P_0 \rangle = \frac{i}{2} \left\{ \frac{4}{3} k_1^3 |\langle 2^3S_1 \| Q_1 \| 2^3P_0 \rangle|^2 \right\}, \quad (2.18)$$

$$\begin{aligned} \langle 2^3P_2 | V_{\text{rd}} | 2^3P_2 \rangle = \frac{i}{2} \left\{ \frac{4}{15} k_1^3 |\langle 2^3S_1 \| Q_1 \| 2^3P_2 \rangle|^2 \right. \\ \left. + \frac{\alpha^2}{225} k_0^5 |\langle 2^1S_0 \| M_2 \| 2^3P_2 \rangle|^2 \right\}, \end{aligned} \quad (2.19)$$

$$\begin{aligned} \langle 2^3P_1 | V_{\text{rd}} | 2^3P_1 \rangle = \frac{i}{2} \left\{ \frac{4}{9} k_0^3 |\langle 1^1S_0 \| Q_1 \| 2^3P_1 \rangle|^2 \right. \\ \left. + \frac{4}{9} k_1^3 |\langle 2^3S_1 \| Q_1 \| 2^3P_1 \rangle|^2 \right\}, \end{aligned} \quad (2.20)$$

$$\begin{aligned} \langle 2^1P_1 | V_{\text{rd}} | 2^1P_1 \rangle = \frac{i}{2} \left\{ \frac{4}{9} k_0^3 |\langle 1^1S_0 \| Q_1 \| 2^1P_1 \rangle|^2 \right. \\ \left. + \frac{4}{9} k_1^3 |\langle 2^3S_1 \| Q_1 \| 2^1P_1 \rangle|^2 \right\}, \end{aligned} \quad (2.21)$$

$$\begin{aligned} \langle 2^3P_1 | V_{\text{rd}} | 2^1P_1 \rangle = \frac{i}{2} \left\{ \frac{4}{9} k_0^3 \langle 1^1S_0 \| Q_1 \| 2^1P_1 \rangle \right. \\ \times \langle 1^1S_0 \| Q_1 \| 2^3P_1 \rangle \\ \left. + \frac{4}{9} k_1^3 \langle 2^3S_1 \| Q_1 \| 2^1P_1 \rangle \right. \\ \left. \times \langle 2^3S_1 \| Q_1 \| 2^3P_1 \rangle \right\}. \end{aligned} \quad (2.22)$$

In these equations, k_0 and k_1 are wave numbers of the transitions from the state of interest (e.g., the 2^3P_0 state) to the 1^1S_0 and 2^3S_1 states, respectively. For the four diagonal

TABLE IV. Hyperfine matrix elements $\langle J' \| \mathcal{T}^{(1)} \| J \rangle \equiv \langle 3J' \| \mathcal{T}^{(1)} \| 3J \rangle$ between 2^3P_J states from the present work are compared with values inferred from the nonrelativistic variational calculations of Aashamar and Hambro [3].

Z	Present calculation				Ref. [3]			
	$\langle 1 \ \mathcal{T}^{(1)} \ 0 \rangle$	$\langle 1 \ \mathcal{T}^{(1)} \ 1 \rangle$	$\langle 1 \ \mathcal{T}^{(1)} \ 2 \rangle$	$\langle 2 \ \mathcal{T}^{(1)} \ 2 \rangle$	$\langle 1 \ \mathcal{T}^{(1)} \ 0 \rangle$	$\langle 1 \ \mathcal{T}^{(1)} \ 1 \rangle$	$\langle 1 \ \mathcal{T}^{(1)} \ 2 \rangle$	$\langle 2 \ \mathcal{T}^{(1)} \ 2 \rangle$
2	0.1078	0.0956	0.1212	0.2119	0.1078	0.0955	0.1212	0.2119
3	0.3591	0.3266	0.4058	0.7170	0.3587	0.3257	0.4061	0.7167
4	0.8475	0.7834	0.9596	1.7074	0.8457	0.7789	0.9611	1.7058
5	1.6539	1.5472	1.8712	3.3485	1.6474	1.5312	1.8768	3.3431
6	2.8606	2.7045	3.2263	5.8064	2.8427	2.6584	3.2439	5.7928
7	4.5528	4.3496	5.1068	9.2486	4.5103	4.2365	5.1529	9.2184
8	6.8187	6.5876	7.5885	13.844	6.7287	6.3416	7.6945	13.784
9	9.7513	9.5384	10.739	19.762	9.5768	9.0495	10.959	19.654
10	13.449	13.340	14.615	27.176	13.133	12.436	15.037	26.990

matrix elements shown here, they can also be expressed in term of the total level width Γ as

$$\begin{aligned} \langle 2 \ ^3P_J | V_{\text{rd}} | 2 \ ^3P_J \rangle &= \frac{i}{2} \Gamma(2 \ ^3P_J) \\ &= \frac{i}{2} \sum_{k\lambda} \sum_n \hbar A_k^{(\lambda)}(2 \ ^3P_J \rightarrow n), \end{aligned} \quad (2.23)$$

where $A_k^{(\lambda)}(2 \ ^3P_J \rightarrow n)$ are multipole transition rates from the unperturbed $2 \ ^3P_J$ state to lower-energy states n given in Eqs. (2.14)–(2.16).

Including V_{rd} together with $H_0 + H_{\text{hf}}$ in Eq. (2.4) leads to a complex generalization of the 4×4 hyperfine energy eigenvalue problem. The real parts of the eigenvalues give the energies of the hyperfine levels while the imaginary parts give the half-widths of the hyperfine lines from which quenching rates can be deduced. For cases where the radiative half-widths of the levels are small compared to the fine-structure intervals, the eigenvalues of the complex matrix reduce precisely to the results of perturbation theory given in the previous section. It should be emphasized that the coherent combinations of the two $J=1$ amplitudes that occur in the limiting case are a consequence of the fact that off-diagonal contributions are included in the complex energy matrix.

TABLE V. Hyperfine structure of the 2^3P levels of ^3He . Energies in MHz relative to the unperturbed $J=0$ level. $\Delta_{J,F} = E_{J,F} - E_{2,5/2}$. Fine-structure energies, $E_J - E_0$, are from Ref. [7].

J	$E_J - E_0$	(J, F)	$E_{J,F}$	$\Delta_{J,F}$	Expt. [7]	Expt. [8]
^3He ($\mu = -2.127\,625$ $I = 1/2$)						
0	0	(0, 1/2)	324	34 384	34 386	34 394
1	-29 617	(1, 3/2)	-27 102	6959	6961	6971
		(1, 1/2)	-27 770	6291	6293	6291
2	-31 908	(2, 3/2)	-32 280	1780	1781	1807
		(2, 5/2)	-34 060			

If we limit our calculation to a 2×2 complex matrix coupling only the 2^3P_0 and 2^3P_1 states, our method essentially reduces to the MCDF approach by Indelicato *et al.* [17] in evaluating the quenching rates for the $J=0$ states. This formulation gives approximately correct quenching rates in the range $Z > 40$ where interference between the $J=1$ amplitudes contributes only a few percent to the decay rate. For lower Z , however, the 2×2 approximation can lead to large errors in the predicted quenching rates.

III. DISCUSSION AND CONCLUSIONS

A. Comparisons with nonrelativistic variational calculations

As mentioned in the Introduction, precise nonrelativistic variational values of the hyperfine constants for 2^3P states of helium and heliumlike ions with $Z \leq 10$ were given in Refs. [2,3]. Numerical values of three hyperfine constants

$$C = -\frac{16\pi}{3} \left\langle \sum_i \delta(\mathbf{r}_i) \right\rangle, \quad (3.1)$$

$$D = -4 \left\langle \sum_i \frac{[\mathbf{r}_i \times \mathbf{p}_i]_z}{r_i^3} \right\rangle, \quad (3.2)$$

$$E = \frac{5}{2} \left\langle \sum_i \frac{r_i^2 - 3z_i^2}{r_i^5} \right\rangle, \quad (3.3)$$

are given in Table 1 of Ref. [3] for $Z = 2, 3, \dots, 10$. Reduced matrix elements of the dipole hyperfine operator between triplet states are expressed in terms of these nonrelativistic hyperfine constants by the relations

$$\langle 31 \| \mathcal{T}^{(1)} \| 30 \rangle = -\alpha \frac{\sqrt{2}}{2} (C - D + 2E), \quad (3.4)$$

$$\langle 31 \| \mathcal{T}^{(1)} \| 31 \rangle = -\alpha \frac{\sqrt{6}}{4} (C + D - 4E), \quad (3.5)$$

$$\langle 31 \| \mathcal{T}^{(1)} \| 32 \rangle = -\alpha \frac{\sqrt{10}}{4} \left(C - D - \frac{8}{5}E \right), \quad (3.6)$$

TABLE VI. Hyperfine structure of the 2^3P levels of ${}^6\text{Li}^+$ and ${}^7\text{Li}^+$. Energies in MHz relative to the unperturbed $J=0$ level. $\Delta_{F,F-1}=E_{J,F}-E_{J,F-1}$. Fine-structure energies, E_J-E_0 , are from Ref. [9].

J	E_J-E_0	(J,F)	$E_{J,F}$	$\Delta_{F,F-1}$	Expt. [9]	Expt. [10]	Ref. [13]
${}^6\text{Li}^+$ ($\mu=0.82205$ $I=1$)							
0	0	(0, 1)	63				
2	-93 023	(2, 3)	-90 209	4126	4125(14)		4127
		(2, 2)	-94 335	2856	2861(6)		2858
		(2, 1)	-97 191				
1	-155 698	(1, 2)	-154 360	2887	2886(4)		2880
		(1, 1)	-157 247	1317	1316(8)		1314
		(1, 0)	-158 564				
${}^7\text{Li}^+$ ($\mu=3.2564$ $I=3/2$)							
0	0	(0, 3/2)	812				
2	-93 019	(2, 7/2)	-81 871	11 770	11 760(6)	11 761(12)	11 770
		(2, 5/2)	-93 642	9602	9598(12)	9603(12)	9606
		(2, 3/2)	-103 244	6199	6204(13)	6182(18)	6204
		(2, 1/2)	-109 443				
1	-155 694	(1, 5/2)	-151 253	9961	9953(9)	9932(24)	9941
		(1, 3/2)	-161 214	4239	4246(20)	4224(18)	4223
		(1, 1/2)	-165 454				

$$\langle 32 || T^{(1)} || 32 \rangle = -\alpha \frac{\sqrt{30}}{4} \left(C + D + \frac{4}{5} E \right). \quad (3.7)$$

In Table IV, we compare values of the reduced matrix elements from the present calculation with those inferred from the nonrelativistic calculations of Ref. [3] using the above formulas. We find excellent agreement at $Z=2$. However, owing to relativistic corrections, differences between the two calculations increase to a few percent as Z increases from 2 to 10.

B. Comparison with experiment for ${}^3\text{He}$, ${}^6,7\text{Li}^+$, and ${}^{19}\text{F}^{7+}$

Values of the nuclear moments used in this work are those given by Raghavan [24]. In cases where several experimental values are reported in Ref. [24], weighted averages are used.

${}^3\text{He}$: Precise measurements of the hyperfine pattern of the 2^3P levels in ${}^3\text{He}$ were carried out in Refs. [7,8]. Using the matrix elements from Table I, together with the experimentally determined fine-structure intervals for ${}^4\text{He}$, $\Delta E_{10} = -29,617$ MHz and $\Delta E_{20} = -31,908$ MHz from Ref.

TABLE VII. Hyperfine structure of the 2^3P levels of ${}^9\text{Be}^{2+}$. Energies in cm^{-1} relative to the unperturbed fine structure levels. $\Delta_F = E_{J,F} - E_{J,F+1}$.

J	E_J-E_0	(J,F)	$E_{J,F}$	Δ_F	Expt. [11]
${}^9\text{Be}^{2+}$ ($\mu=-1.1775$ $I=3/2$)					
0	0	(0, 3/2)	0.0092		
1	-11.54	(1, 1/2)	0.2728	0.1754	0.1751(10)
		(1, 3/2)	0.0974	0.2654	0.2654(10)
		(1, 5/2)	-0.1680		
2	3.29	(2, 1/2)	0.4811	0.1581	0.1585(10)
		(2, 3/2)	0.3230	0.2659	0.2659(11)
		(2, 5/2)	0.0571	0.3773	0.3768(14)
		(2, 7/2)	-0.3202		

[7], we obtain the hyperfine intervals listed in the third column of Table V. These values are seen to be in excellent agreement with the measured intervals given in the sixth and seventh columns. Coupling to the 2^1P_1 state does not influence the predicted hyperfine pattern at the 0.1-MHz level of accuracy.

${}^{6,7}\text{Li}^+$: Measurements of the hyperfine pattern of the 2^3P levels in ${}^{6,7}\text{Li}^+$ were carried out in Refs. [9,10]. Using the matrix elements from Table I, together with the experimentally determined fine-structure intervals given in Ref. [9], we obtain the hyperfine intervals listed in the fourth column of Table VI. These are seen to be in excellent agreement with the measurements [9,10], which are given in the sixth and seventh columns, and also with the coupled-cluster calculations of Ref. [13], which are given in the eighth column. Again, coupling to the 2^1P_1 state was unimportant at the level of accuracy in this table.

${}^9\text{Be}^{2+}$: Energies of the 2^3P levels in ${}^9\text{Be}^{2+}$ were measured to high accuracy in Ref. [11]. From these measurements, one can infer the experimental hyperfine intervals $\Delta_F = E_{J,F} - E_{J,F+1}$ listed in the last column of Table VII. The measured intervals agree to within the experimental errors with the values from the present calculation.

TABLE VIII. Hyperfine structure of the 2^3P levels of ${}^{19}\text{F}^{7+}$. Energies in cm^{-1} relative to the unperturbed $J=0$ level. $\Delta_F = E_{2,F} - E_{1,F-1}$.

J	E_J-E_0	(J,F)	$E_{J,F}$	Δ_F	Expt. [12]
${}^{19}\text{F}^{7+}$ ($\mu=2.6289$ $I=1/2$)					
0	0	(0, 1/2)	-0.87		
1	151.28	(1, 1/2)	143.22		
		(1, 3/2)	155.66		
2	1109.15	(2, 3/2)	1096.82	953.60	953.60(3)
		(2, 5/2)	1117.42	961.76	961.77(3)

TABLE IX. Hyperfine energies $E_{J,F}$ and weight coefficients $C_{\gamma J}^I$ of the $(J,F)=(0,I)$ hyperfine level for several He-like ions. The values of $E_{0,I}$ are relative to the unperturbed $J=0$ level in cm^{-1} . Numbers in brackets represent powers of ten.

Ion	I	μ_I	$E_{0,I}$	C_{30}^I	C_{31}^I	C_{32}^I	C_{11}^I
^{19}F	1/2	2.6289	-0.8742	9.9697[-1]	-7.7835[-2]	0	1.7065[-4]
^{23}Na	3/2	2.2176	-0.3266	9.9969[-1]	-2.5044[-2]	-6.6865[-5]	1.3395[-4]
^{27}Al	5/2	3.6415	-0.8732	9.9965[-1]	-2.6449[-2]	-8.3207[-5]	2.5691[-4]
^{31}P	1/2	1.1316	-0.2288	9.9995[-1]	-9.6973[-3]	0	1.4187[-4]

$^{19}\text{F}^{7+}$: Two energy intervals between the (J,F) levels in the hyperfine pattern of the 2^3P state, $\Delta_F = E_{2,F} - E_{1,F-1}$, were measured in Ref. [12]. The measured energy intervals, $\Delta_{3/2} = 953.60(3)$ MHz and $\Delta_{5/2} = 961.77(3)$ MHz, agree precisely with the values, $\Delta_{3/2} = 953.60$ MHz and $\Delta_{5/2} = 961.76$ MHz, from the present calculation as shown in Table VIII, where we present the complete 2^3P hyperfine pattern for $^{19}\text{F}^{7+}$.

C. Hyperfine quenching

In Table IX, we list the $J=0$ level shifts and the corresponding expansion coefficients $C_{\gamma J}^I$ for the four ions, $^{19}\text{F}^{7+}$, $^{23}\text{Na}^{9+}$, $^{27}\text{Al}^{11+}$, and $^{31}\text{P}^{13+}$, obtained by solving the eigenvalue equation (2.4) in the special case $F=I$. To obtain accurate quenching rates for low and intermediate Z ions, it is crucial to include the coupling with the 2^1P_1 state. Although this state has small weight, as seen in the table, it does have a large transition amplitude to the ground state. Moreover, the amplitudes for transitions from the 2^3P_1 and 2^1P_1 states add coherently to give the hyperfine quenching rate to the ground state. The importance of the 2^1P_1 state is illustrated in Fig. 1, where we plot the percentage difference in quenching rates calculated with and without the singlet-state contributions. This ratio has a maximum value of about 40% near $Z=14$, and decreases to less than 1% at $Z=40$.

1. $Z = 6-40$

Hyperfine quenching of 2^3P_0 states for heliumlike ions was carried out in the relativistic $1/Z$ approximation by Mohr [15]. These calculations included contributions from the contact interaction C in Eq. (3.1) only. Similar calculations, using MCHF wave functions with Breit-Pauli corrections and

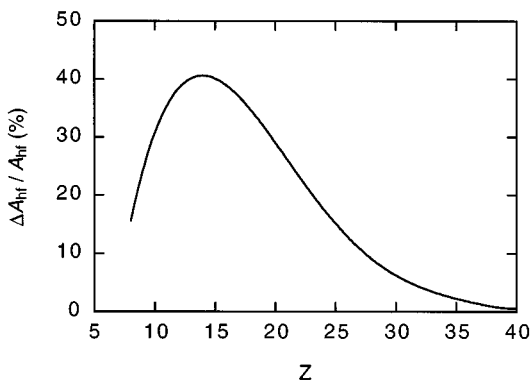


FIG. 1. Percentage change in the theoretical hyperfine quenching rate A_{hf} when contributions from the 2^1P_1 state are included.

including contributions from all three hyperfine constants C , D , and E of Eqs. (3.1)–(3.3), were carried out by Aboussaïd *et al.* [16].

In Table X, we present the values of the unperturbed transition rates A_0 , the hyperfine induced rate A_{hf} , and the resulting 2^3P_0 lifetime τ in the range of $Z=6-40$ calculated using the radiation-damping formalism from the previous section. For $Z \leq 32$ these values agree to four significant figures with results obtained using perturbation theory. For $Z=40$, the difference between radiation-damping theory and perturbation theory increases to 1.5%.

The transition amplitudes used in this calculation were obtained from the line strengths tabulated in Ref. [6], which were also evaluated using relativistic CI wave functions. In Table X, we also compare the present values of A_{hf} with those obtained from the relativistic $1/Z$ expansion of Mohr [15] for $Z = 9, 11, \dots, 29$, and with the MCHF calculations of Aboussaïd *et al.* [16] for $Z = 9, 11$, and 13. The present rates are 2–3% smaller than those from Ref. [16], presumably because of higher-order relativistic corrections. They disagree with the $1/Z$ values from Ref. [15] by as much as 5%.

We also include in this table experimental lifetimes for ^{19}F [25,26], ^{27}Al [27], ^{31}P [28,29], and ^{61}Ni [18]. These measurements, which are consistent with the theory for all of the cases listed, clearly establish the fact that hyperfine quenching occurs.

2. $Z = 41-60$

For He-like ions with $Z > 40$, coupling to the 2^1P state is relatively unimportant as is apparent from Fig. 1. However,

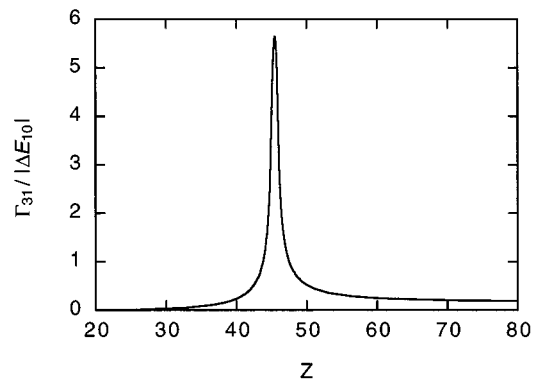


FIG. 2. Ratio of the full width of the 2^3P_1 state Γ_{31} to the fine-structure interval $|\Delta E_{10}|$ plotted as a function of Z . The peak between $Z=45$ and $Z=46$ corresponds the level crossing between the 2^3P_1 and 2^3P_0 states ($|\Delta E_{10}|=0$).

TABLE X. Hyperfine quenching of 2^3P_0 levels of heliumlike ions with nuclear charges in the range $Z=6-40$. In column 5, A_0 is the unperturbed decay rate of the 2^3P_0 state in ns^{-1} from Ref. [6]. In columns 6-8, the values of the hyperfine-induced $2^3P_0 \rightarrow 1^1S_0$ transition rates are shown in ns^{-1} , where A_{hf} is the result of this work, $A_{\text{hf}}(1/Z)$ is from the relativistic $1/Z$ expansion calculations of Mohr [15], and $A_{\text{hf}}(\text{HF})$ is from the MCHF calculations of Aboussaïd *et al.* [16]. In the last two columns, τ is the quenched lifetime of the 2^3P_0 state in ns.

Ion	Z	μ_I	I	$A_0(\text{ns}^{-1})$	$A_{\text{hf}}(\text{ns}^{-1})$	$A_{\text{hf}}(1/Z)$	$A_{\text{hf}}(\text{HF})$	$\tau(\text{ns})$	τ_{Expt}
^{13}C	6	0.70241	1/2	0.05652	0.00011			17.66	
^{14}N	7	0.40376	1	0.06770	0.00086			14.59	
^{15}N	7	-0.28319	1/2	0.06770	0.00054			14.65	
^{17}O	8	-1.8938	5/2	0.07902	0.00260			12.25	
^{19}F	9	2.6289	1/2	0.09054	0.01391	0.013	0.0142	9.574	9.48(20) ^a
^{21}Ne	10	-0.6618	3/2	0.1023	0.0006			9.714	
^{23}Na	11	2.2176	3/2	0.1143	0.0119	0.012	0.0122	7.922	
^{25}Mg	12	-0.85545	5/2	0.1266	0.0024			7.751	
^{27}Al	13	3.6415	5/2	0.1393	0.0737	0.074	0.0760	4.695	4.8(2) ^b
^{29}Si	14	-0.55529	1/2	0.1524	0.0059			6.317	
^{31}P	15	1.1316	1/2	0.1659	0.0409	0.041		4.836	4.88(9) ^c
^{33}S	16	0.64382	3/2	0.1799	0.0116			5.223	
^{35}Cl	17	0.82187	3/2	0.1944	0.0297	0.030		4.462	
^{36}Cl	17	1.28547	2	0.1944	0.0655			3.848	
^{37}Cl	17	0.68412	3/2	0.1944	0.0206			4.652	
^{39}K	19	0.39149	3/2	0.2250	0.0160	0.016		4.149	
^{40}K	19	-1.2981	4	0.2250	0.1317			2.804	
^{41}K	19	0.21488	3/2	0.2250	0.0048			4.351	
^{41}Ca	20	-1.5948	7/2	0.2412	0.3095			1.816	
^{43}Ca	20	-1.3176	7/2	0.2412	0.2114			2.209	
^{45}Sc	21	4.7565	7/2	0.2581	4.181	4.15		0.2253	
^{47}Ti	22	-0.78848	5/2	0.2758	0.1836			2.177	
^{49}Ti	22	-1.1042	7/2	0.2758	0.3307			1.649	
^{50}V	23	3.3457	6	0.2941	4.084			0.2284	
^{51}V	23	5.1487	7/2	0.2941	10.73	10.5		0.09075	
^{53}Cr	24	-0.47454	3/2	0.3134	0.1705			2.066	
^{51}Mn	25	3.5683	5/2	0.3335	11.93			0.08154	
^{55}Mn	25	3.4687	5/2	0.3335	11.27	10.7		0.08618	
^{57}Fe	26	0.09062	1/2	0.3545	0.0236			2.645	
^{59}Co	27	4.627	7/2	0.3765	38.32	36.0		0.02584	
^{61}Ni	28	-0.75002	3/2	0.3996	1.845			0.4455	0.470(50) ^d
^{63}Cu	29	2.2273	3/2	0.4239	23.80	21.7		0.04128	
^{65}Cu	29	2.3816	3/2	0.4239	27.24			0.03615	
^{67}Zn	30	0.8752	5/2	0.4493	4.373			0.2074	
^{69}Ga	31	2.0166	3/2	0.4760	40.17			0.02460	
^{71}Ga	31	2.5623	3/2	0.4760	65.12			0.01525	
^{73}Ge	32	0.87947	9/2	0.5040	7.911			0.1188	
^{75}As	33	1.4395	3/2	0.5335	42.50			0.02324	
^{77}Se	34	0.53504	1/2	0.5646	15.45			0.06246	
^{79}Br	35	2.1064	3/2	0.5972	196.9			0.005065	
^{81}Br	35	2.2706	3/2	0.5972	229.2			0.004353	
^{83}Kr	36	0.97067	9/2	0.6316	44.30			0.02226	
^{85}Rb	37	1.3534	5/2	0.6678	152.0			0.006551	
^{87}Rb	37	2.7515	3/2	0.6678	768.7			0.001300	
^{87}Sr	38	1.0936	9/2	0.7059	131.7			0.007555	
^{89}Y	39	0.13742	1/2	0.7460	8.139			0.1126	
^{91}Zr	40	-1.3036	5/2	0.7884	561.6			0.001778	

^aEngström *et al.* [25,26].

^bDenne *et al.* [27].

^cLivingston and Hinterlong [28], Vogel Vogt [29].

^dDunford *et al.* [18].

TABLE XI. Hyperfine quenching of 2^3P_0 levels of heliumlike ions with nuclear charges in the range $Z=41-60$. Here, A_0 is the unperturbed decay rate of the 2^3P_0 state in ns^{-1} from Ref. [6], A_{hf} is the hyperfine-induced $2^3P_0 \rightarrow 1^1S_0$ transition rates in ps^{-1} of this work, and τ is the quenched lifetime of the 2^3P_0 state in ps, also of this work. The last column gives comparison values of the quenched lifetime, $\tau(\text{MCDF})$, from the MCDF calculations of Indelicato *et al.* [17].

Ion	Z	μ_I	I	A_0 (ns^{-1})	A_{hf} (ps^{-1})	$\tau(\text{ps})$	$\tau(\text{MCDF})$
^{93}Nb	41	6.1705	9/2	0.8328	19.77	0.05057	
^{95}Mo	42	-0.9142	5/2	0.8799	0.9406	1.062	1.058
^{97}Mo	42	-0.9335	5/2	0.8799	0.9801	1.019	1.014
^{99}Tc	43	5.6847	9/2	0.9295	67.21	0.01488	0.01885
^{99}Ru	44	-0.6413	5/2	0.9819	2.820	0.3545	0.3899
^{101}Ru	44	-0.7188	5/2	0.9819	3.525	0.2836	0.3235
^{103}Rh	45	-0.08840	1/2	1.037	0.3820	2.611	2.773
^{105}Pd	46	-0.642	5/2	1.095	9.656	0.1036	0.1022
^{107}Ag	47	-0.11368	1/2	1.157	0.2674	3.724	3.608
^{109}Ag	47	-0.13069	1/2	1.157	0.3548	2.810	2.744
^{111}Cd	48	-0.59489	1/2	1.222	4.112	0.2431	0.2262
^{113}Cd	48	-0.6223	1/2	1.222	4.520	0.2212	0.2058
^{113}In	49	5.5289	9/2	1.290	69.23	0.01444	0.01167
^{115}In	49	5.5408	9/2	1.290	69.49	0.01439	0.01162
^{115}Sn	50	-0.91883	1/2	1.363	4.554	0.2195	0.1576
^{117}Sn	50	-1.0010	1/2	1.363	5.454	0.1833	0.1714
^{119}Sn	50	-1.0473	1/2	1.363	6.000	0.1666	0.2011
^{121}Sb	51	-3.3634	5/2	1.439	21.12	0.04735	0.04543
^{123}Sb	51	2.5498	7/2	1.439	10.18	0.09824	0.08773
^{123}Te	52	-0.73695	1/2	1.519	1.852	0.5396	0.5924
^{125}Te	52	-0.8885	1/2	1.519	2.726	0.3666	0.4133
^{127}I	53	2.8133	5/2	1.605	9.754	0.1025	0.09093
^{129}Xe	54	-0.77798	1/2	1.695	1.600	0.6243	0.6780
^{131}Xe	54	0.69186	3/2	1.695	0.6543	1.525	1.433
^{133}Cs	55	2.5826	7/2	1.790	6.390	0.1565	0.1322
^{135}Ba	56	0.83863	3/2	1.891	0.8290	1.203	1.137
^{137}Ba	56	0.93735	3/2	1.891	1.033	0.9658	0.9075
^{138}La	57	3.7136	5	1.997	11.02	0.09075	0.08521
^{139}La	57	2.7830	7/2	1.997	6.642	0.1505	0.1407
^{141}Pr	59	4.2754	5/2	2.228	15.64	0.06392	0.06048
^{143}Nd	60	-1.065	7/2	2.353	0.9324	1.070	1.067
^{145}Nd	60	-0.656	7/2	2.353	0.3528	2.815	2.799

in this range of Z , the radiative width of the 2^3P_1 state Γ_{31} is comparable to the energy separation between the 2^3P_1 and 2^3P_0 states, ΔE_{10} . (Here, $\Gamma_{\gamma J} = \hbar A_{\gamma J}$, where $A_{\gamma J}$ is the total decay rate of the $2^{\gamma}P_J$ state.) This fact is illustrated in Fig. 2, where we plot the ratio $\Gamma_{31}/\Delta E_{10}$ as a function of Z . The peak in this curve between $Z=45$ and 46 corresponds to a sign change in ΔE_{10} (the level crossing between the 2^3P_1 and 2^3P_0 states) that can be seen in the second column of Table III. For $Z=41-60$, it is, therefore, necessary to treat radiative transitions on an equal footing with the hyperfine interaction, as with the present radiation-damping method. In Table XI, we present the unperturbed decay rates A_0 , the perturbation corrections A_{hf} , and the resulting lifetimes τ , for 2^3P_0 states of heliumlike ions with $Z=41-60$. We compare these rates with the MCDF values

TABLE XII. Hyperfine quenching of 2^3P_0 levels of heliumlike ions with nuclear charges in the range $Z=62-92$. Here, A_0 is the unperturbed decay rate of the 2^3P_0 state in ns^{-1} from Ref. [6], A_{hf} is the hyperfine-induced $2^3P_0 \rightarrow 1^1S_0$ transition rates in ps^{-1} of this work, and τ is the quenched lifetime of the 2^3P_0 state in ps, also of this work. The last column gives comparison values of the quenched lifetime, $\tau(\text{MCDF})$, from the MCDF calculations of Indelicato *et al.* [17].

Ion	Z	μ_I	I	A_0 (ns^{-1})	A_{hf} (ps^{-1})	$\tau(\text{ps})$	$\tau(\text{MCDF})$
^{147}Sm	62	-0.8148	7/2	2.623	0.5385	1.848	2.012
^{149}Sm	62	-0.6715	7/2	2.623	0.3654	2.717	2.952
^{151}Eu	63	3.4717	5/2	2.768	10.26	0.09745	0.09045
^{153}Eu	63	1.5330	5/2	2.768	2.043	0.4888	0.4690
^{155}Gd	64	-0.2581	3/2	2.925	0.07078	13.57	13.41
^{157}Gd	64	-0.3386	3/2	2.925	0.1220	8.008	7.938
^{159}Tb	65	2.014	3/2	3.090	4.224	0.2366	0.2213
^{161}Dy	66	-0.4804	5/2	3.263	0.2124	4.637	4.571
^{163}Dy	66	0.6726	5/2	3.263	0.4124	2.406	2.319
^{165}Ho	67	4.173	7/2	3.446	14.51	0.06888	0.06641
^{167}Er	68	-0.56385	7/2	3.638	0.2805	3.519	0.03770
^{169}Tm	69	-0.2316	1/2	3.839	0.1140	8.487	8.568
^{171}Yb	70	0.4937	1/2	4.049	0.5175	1.917	1.015
^{173}Yb	70	-0.6799	5/2	4.049	0.4692	2.113	2.121
^{175}Lu	71	2.238	7/2	4.273	4.731	0.2112	0.2052
^{176}Lu	71	3.1692	7	4.273	8.453	0.1182	0.1141
^{177}Hf	72	0.7935	7/2	4.507	0.6192	1.603	1.583
^{179}Hf	72	-0.6409	9/2	4.507	0.3867	2.556	2.561
^{181}Ta	73	2.3705	7/2	4.754	5.676	0.1760	0.1729
^{183}W	74	0.11778	1/2	5.011	0.03414	25.54	25.39
^{185}Re	75	3.1871	5/2	5.287	11.88	0.08414	0.08033
^{187}Re	75	3.2197	5/2	5.287	12.12	0.08247	0.07872
^{187}Os	76	0.064652	1/2	5.574	0.01114	59.83	59.43
^{189}Os	76	0.65993	3/2	5.574	0.6411	1.546	1.522
^{191}Ir	77	0.1484	3/2	5.875	0.03401	25.07	25.64
^{193}Ir	77	0.1614	3/2	5.875	0.04022	21.70	22.16
^{195}Pt	78	0.60952	1/2	6.187	1.054	0.9433	0.9167
^{197}Au	79	0.14816	3/2	6.515	0.03688	23.04	23.66
^{199}Hg	80	0.50588	1/2	6.852	0.7941	1.248	1.209
^{201}Hg	80	-0.56022	3/2	6.852	0.5543	1.782	1.811
^{203}Tl	81	1.6222	1/2	7.215	8.225	0.1215	0.1091
^{205}Tl	81	1.6382	1/2	7.215	8.383	0.1192	0.1069
^{207}Pb	82	0.59258	1/2	7.663	1.189	0.8357	0.8345
^{209}Bi	83	4.1106	9/2	7.971	24.50	0.04080	0.03971
^{223}Ra	88	0.2705	3/2	10.04	0.1868	5.079	
^{229}Th	90	0.46	5/2	10.93	0.5007	1.955	
^{235}U	92	-0.39	7/2	11.81	0.3695	2.623	2.145
^{239}Pu	94	0.203	1/2	12.67	0.2571	3.707	

from Ref. [17] and find differences of up to 10% in this range of nuclear charge. These differences are in part due to differences in the sign of the hyperfine contribution to the energy matrix. As an example, in the present calculation of the hyperfine matrix for ^{107}Ag , we find $W_{31,30} = -0.01224$ and $W_{31,31} = 0.01533$; whereas the corresponding values from Ref. [19] are $W_{31,30} = -0.01222$ and $W_{31,31} = -0.01531$. (Fine-structure contributions to the diagonal matrix elements are omitted here.) Differences in the signs of the off-diagonal

TABLE XIII. 2^3P_2 hyperfine quenching rates A_{hf} for He-like ions having lifetimes $\tau > 1$ ps, for which hyperfine quenching increases the unperturbed $E1 + M2$ decay rates A_0 by more than 5%.

Ion	Z	μ_I	I	$A_0(\text{ns}^{-1})$	$A_{\text{hf}}(\text{ns}^{-1})$	τ (ps)	% change
^{45}Sc	21	4.7565	7/2	1.693	0.3928	479.5	23
^{50}V	23	3.3457	6	3.188	0.3622	281.7	11
^{51}V	23	5.1487	7/2	3.188	0.9453	242.0	29
^{51}Mn	25	3.5683	5/2	5.891	0.9584	146.0	16
^{55}Mn	25	3.4687	5/2	5.891	0.9056	147.1	15
^{59}Co	27	4.627	7/2	10.59	2.733	75.04	25
^{63}Cu	29	2.2273	3/2	18.49	1.453	50.14	7
^{65}Cu	29	2.3816	3/2	18.49	1.662	49.63	8
^{69}Ga	31	2.0166	3/2	31.31	2.035	29.99	6
^{71}Ga	31	2.5623	3/2	31.31	3.285	28.90	10
^{79}Br	35	2.1064	3/2	82.74	5.908	11.28	7
^{81}Br	35	2.2706	3/2	82.74	6.865	11.16	8
^{87}Rb	37	2.7515	3/2	129.6	15.83	6.876	12
^{93}Nb	41	6.1705	9/2	298.5	134.9	2.307	45
^{99}Tc	43	5.6847	9/2	440.6	169.3	1.640	38

terms can reflect different phase conventions for wave functions and have no physical significance. Differences in the sign of the diagonal matrix elements, on the other hand, indicate a sign difference in the hyperfine interaction Hamiltonian and cannot be ignored. Since the fine-structure interval, which is also on the diagonal of the interaction matrix, is ordinarily much larger than the hyperfine interaction, such an error can easily be overlooked. The only experimental lifetimes in this range of nuclear charge are for ^{107}Ag and ^{109}Ag from the measurements of Ref. [19]. The measured values are $\tau(107) = 3.98(37)$ ps and $\tau(109) = 2.84(32)$ ps, which are consistent with our values of $\tau(107) = 3.72$ ps and $\tau(109) = 2.81$ ps shown in Table XI. They are also consistent with the MCDF values of $\tau(107) = 3.61$ ps and $\tau(109) = 2.74$ ps [17] in spite of the above-mentioned sign errors.

3. $Z = 61-92$

In this range of Z , coupling with the 2^1P_1 state is unimportant and the radiative width of the 2^3P_1 state is again small compared to the energy separation ΔE_{10} . Nevertheless, we continue to use the radiation-damping method and extract the lifetime from the imaginary part of the $J=0$ eigenvalue of the 4×4 complex energy matrix, as perturbation results are off by about 1% in this range. In Table XII, we present results on the unperturbed decay rates A_0 , the perturbation corrections A_{hf} , and lifetimes τ for 2^3P_0 states. Again, we compare the rates with the MCDF values from Ref. [17] and find differences ranging from 0 to 100%. Measured lifetimes are available for ^{155}Gd and ^{157}Gd from Ref. [14]. These values are $\tau(155) = 13.43(27)$ ps and $\tau(157) = 7.65(55)$ ps, which are to be compared with our values of $\tau(155) = 13.57$ ps and $\tau(157) = 8.01$ ps shown in Table XII, and with the MCDF values of $\tau(155) = 13.41$ ps and $\tau(157) = 7.94$ ps from Ref. [14].

D. Hyperfine quenching of 2^3P_2 levels

On p. 293 of Ref. [6], detailed comparisons of theoretical 2^3P_2 decay rates with experiment were given. The theoret-

ical rates change somewhat when hyperfine mixing is considered, but for most of the ions considered in Ref. [6], experimental errors mask the hyperfine quenching corrections. One exception is $^{63}\text{Cu}^{27+}$, where the measured 2^3P_2 lifetime of 47 ± 5 ps as reported in Ref. [30] is in clear disagreement with the unperturbed theoretical value of 54.1 ps from Ref. [6], but is consistent with the quenched lifetime of 50.1 ps obtained from the present calculation. In this case hyperfine quenching changed the unperturbed rate by 7%, while for the other $J=2$ decays considered in Ref. [6], the hyperfine corrections are 1% or less. As a guide for future measurements, we present in Table XIII a list of He-like ions for which hyperfine mixing changes the unperturbed 2^3P_2 decay rates by more than 5%, and for which $\tau > 1$ ps.

E. Bohr-Weisskopf effect

For heavy elements, the distribution of magnetism inside the nucleus gives small corrections to hyperfine constants that were studied many years ago by Bohr and Weisskopf [31]. To estimate the influence of the Bohr-Weisskopf corrections on 2^3P_0 quenching rates, we considered the case of $^{197}\text{Au}^{77+}$ using the model of a uniformly magnetized ball of radius R to describe the nuclear magnetic-moment distribution. This model leads to the replacement $1/r^2 \rightarrow r/R^3$ for $r < R$ in the expression (2.12) for $t_\lambda^{(1)}(\mathbf{r})$. For $^{197}\text{Au}^{77+}$, we used the value $R = 7.019$ fm from Ref. [32] and found a reduction of 1.6–1.8% in the eight reduced matrix elements of $\mathcal{T}^{(1)}$. The corresponding increase in the 2^3P_0 quenched lifetime was 3%. Since the reduced matrix elements are dominated by contributions from the $1s$ electron, we expect that finite-size corrections will scale as the product ZR for other ions.

F. Redetermination of ΔE_{10}

In view of the differences between the present calculation and earlier calculations, we reevaluate the fine-structure intervals ΔE_{10} inferred from quenching experiments using the present matrix elements.

^{61}Ni : The lifetime of the 2^3P_0 state in ^{61}Ni measured in Ref. [18] was $\tau = 0.470(50)$ ns. If we let ΔE_{10} be an adjustable parameter in our calculation, we find that $\Delta E_{10} = 2.40(17)$ eV corresponds to the measured lifetime. The value deduced in Ref. [18] was $\Delta E_{10} = 2.33(15)$ eV, while the theoretical value used in the present calculation (which is expected to be more accurate than either of these two experimentally derived numbers) is 2.323 eV from Table III.

$^{107,109}\text{Ag}$: The lifetimes of the 2^3P_0 states in ^{107}Ag and ^{109}Ag were found to be $\tau = 3.98(37)$ and $2.84(32)$ ps, respectively, in Ref. [19]. From these two measurements, we infer $\Delta E_{10} = -0.84(5)$ and $-0.81(6)$ eV, respectively. A weighted average of these two values gives $\Delta E_{10} = -0.82(4)$ eV, which can be compared to the value $\Delta E_{10} = -0.79(4)$ eV deduced in Ref. [19], and the present theoretical value $\Delta E_{10} = -0.801$ eV from Table III.

$^{155,157}\text{Gd}$: The lifetimes of the 2^3P_0 states in ^{155}Gd and ^{157}Gd were found to be $\tau = 13.43(27)$ and $7.65(55)$ ps, respectively, in the experiments of Ref. [14]. From these two measurements, we infer $\Delta E_{10} = -18.47(20)$ and

–18.14(67) eV, respectively. The weighted average of these two values is $\Delta E_{10} = -18.44(19)$ eV, compared to the value $\Delta E_{10} = -18.57(19)$ eV from Ref. [14], and the present theoretical value $E_{10} = -18.57$ eV from Table III.

In summary, accurate hyperfine matrix elements between substates of the $2^{1,3}P$ states have been determined for all ions from $Z=2$ to $Z=100$ using relativistic CI wave functions that include both Coulomb and Breit interactions. These matrix elements can be used to predict accurate hyperfine energies for 2^3P_J states. Applications to the hyperfine structure of the 2^3P_J states for the ions ^3He , $^6,7\text{Li}^+$, $^9\text{Be}^{2+}$, and $^{19}\text{F}^{7+}$ led to agreement between theory and experiment at the level of experimental uncertainty. The theory of hyperfine quenching was reformulated using a method adopted from radiation-damping theory. This method was designed to treat cases where radiative level widths are comparable to level separations; but, in contrast to methods used previously, reduces properly to perturbation theory for small level widths. Applications were given to predict hyper-

fine quenching rates of the $J=0$ states for all stable ions in the interval $Z=6-92$. Quenching rates for 2^3P_2 states were also presented for ions of possible experimental interest. The calculations presented here provide benchmark values for future measurements of the hyperfine structure of 2^3P_J levels or for hyperfine quenching experiments.

ACKNOWLEDGMENTS

The work of W.R.J. was supported in part by NSF Grant No. PHY 95-13179. The work of K.T.C. was performed under the auspices of the U.S. Department of Energy by Lawrence Livermore National Laboratory under Contract No. W-7405-ENG-48. The authors owe a debt of gratitude to K. Aashamar for helpful remarks concerning the variational calculations. Thanks are also due to H.G. Berry for several useful comments on the manuscript and to P. Indelicato for verifying that the sign of the diagonal matrix element found here is correct.

-
- [1] A. Lurio, M. Mandel, and R. Novick, *Phys. Rev.* **126**, 1758 (1962).
- [2] L. Hambro, *Phys. Rev.* **175**, 31 (1968).
- [3] K. Aashamar and L. Hambro, *J. Phys. B* **10**, 553 (1977).
- [4] M. H. Chen, K. T. Cheng, and W. R. Johnson, *Phys. Rev. A* **47**, 3692 (1993).
- [5] K. T. Cheng, M. H. Chen, W. R. Johnson, and J. Sapirstein, *Phys. Rev. A* **50**, 247 (1994).
- [6] W. R. Johnson, D. R. Plante, and J. Sapirstein, in *Advances in Atomic, Molecular, and Optical Physics*, edited by B. Bederson and H. Walther (Addison-Wesley, New York, 1995), Vol. 35, pp. 255–329.
- [7] J. D. Prestage, E. A. Hinds, and F. M. J. Pichanick, *Phys. Rev. Lett.* **50**, 828 (1983).
- [8] R. R. Freeman, P. F. Liao, R. Panock, and L. M. Humphrey, *Phys. Rev. A* **22**, 1510 (1980).
- [9] R. Bayer, J. Kowalski, R. Neumann, S. Noehte, H. Suhr, K. Winkler, and G. zu Putlitz, *Z. Phys. A* **292**, 329 (1979).
- [10] B. Fan, A. Lurio, and D. Grischkowsky, *Phys. Rev. Lett.* **41**, 1460 (1978).
- [11] T. J. Scholl, R. Cameron, S. D. Rosner, L. Zhang, R. A. Holt, C. J. Sansonetti, and J. D. Gillaspay, *Phys. Rev. Lett.* **71**, 2188 (1993).
- [12] E. G. Myers, P. Kuske, H. J. Andrä, I. A. Armour, N. A. Jelley, H. A. Klein, J. D. Silver, and E. Träbert, *Phys. Rev. Lett.* **47**, 87 (1981).
- [13] A. N. Jette, T. Lee, and T. P. Das, *Phys. Rev. A* **9**, 2337 (1974).
- [14] P. Indelicato, B. B. Birkett, J. P. Briand, P. Charles, D. D. Dietrich, R. Marrus, and A. Simionovici, *Phys. Rev. Lett.* **68**, 1307 (1992).
- [15] P. J. Mohr, in *Beam-Foil Spectroscopy, Atomic Structure, and Lifetimes*, edited by I. Sellin and D. J. Pegg (Plenum, New York, 1976), Vol. 1, pp. 97–103.
- [16] A. Aboussaïd, M. R. Godefroid, P. Jönsson, and C. F. Fischer, *Phys. Rev. A* **51**, 2031 (1995).
- [17] P. Indelicato, F. Parente, and R. Marrus, *Phys. Rev. A* **40**, 3505 (1989).
- [18] R. W. Dunford, C. J. Liu, J. Last, N. Berrah-Mansour, R. Vondrasek, D. A. Church, and L. J. Curtis, *Phys. Rev. A* **44**, 764 (1991).
- [19] R. Marrus, A. Simionovici, P. Indelicato, D. D. Dietrich, P. Charles, J. P. Briand, K. Finlayson, F. Bosch, D. Liesen, and F. Parente, *Phys. Rev. Lett.* **63**, 502 (1989).
- [20] A. J. Akhiezer and V. B. Berestetskii, *Quantum Electrodynamics* (Interscience, New York, 1965), Chap. 1, Sec. 4.2.
- [21] K. T. Cheng and W. J. Childs, *Phys. Rev. A* **31**, 2775 (1985).
- [22] G. W. Drake, *Can. J. Phys.* **66**, 586 (1988).
- [23] F. Robicheaux, T. W. Gorczyca, M. S. Pindzola, and N. R. Badnell, *Phys. Rev. A* **52**, 1319 (1995).
- [24] P. Raghavan, *At. Data Nucl. Data Tables* **42**, 189 (1989).
- [25] L. Engström, C. Jupén, B. Denne, S. Huldt, T. M. Weng, P. Kaijser, U. Litzén, and I. Martinson, *J. Phys. B* **13**, L143 (1980).
- [26] L. Engström, C. Jupén, B. Denne, S. Huldt, T. M. Weng, P. Kaijser, J. O. Ekberg, U. Litzén, and I. Martinson, *Phys. Scr.* **22**, 570 (1981).
- [27] B. Denne, S. Huldt, J. Pihl, and R. Hallin, *Phys. Scr.* **22**, 45 (1980).
- [28] A. E. Livingston and S. J. Hinterlong, *Nucl. Instrum. Methods* **202**, 103 (1982).
- [29] C. Vogel Vogt (unpublished).
- [30] J. P. Buchet, M. C. Buchet-Poulizac, A. Denis, J. Désesquelles, M. Dreutta, J.P. Grandin, X. Husson, D. Lecler, and H. F. Beyer, *Nucl. Instrum. Methods B* **9**, 645 (1985).
- [31] A. Bohr and V. F. Weisskopf, *Phys. Rev.* **77**, 94 (1951).
- [32] W. R. Johnson and G. Soff, *At. Data Nucl. Data Tables* **33**, 405 (1985).